Supplementary Information (SI) for Journal of Materials Chemistry A.
This journal is © The Royal Society of Chemistry 2026

Supporting information

Achieving the directional zinc ions transport in belt-like orderly arranged vanadium dioxide cathode material

Siyang Han[1], Hongxu, Zhou[1], Weichen Han[1], Jingang Zheng[1], Hongwei Zhao[1], Lixiang Li[1], Baigang An[1] and Chengguo Sun[1,2*]*

[1] School of Chemical Engineering, University of Science and Technology Liaoning, Anshan 114051, P. R. China
[2] School of Chemical Engineering, Nanjing University of Science and Technology, Nanjing, Jiangsu 210094, P. R. China

*Corresponding author.
E-mail address: bgan@ustl.edu.cn (Baigang An), sunyangguo2004@163.com (Chengguo Sun)

1. Supplementary Figures

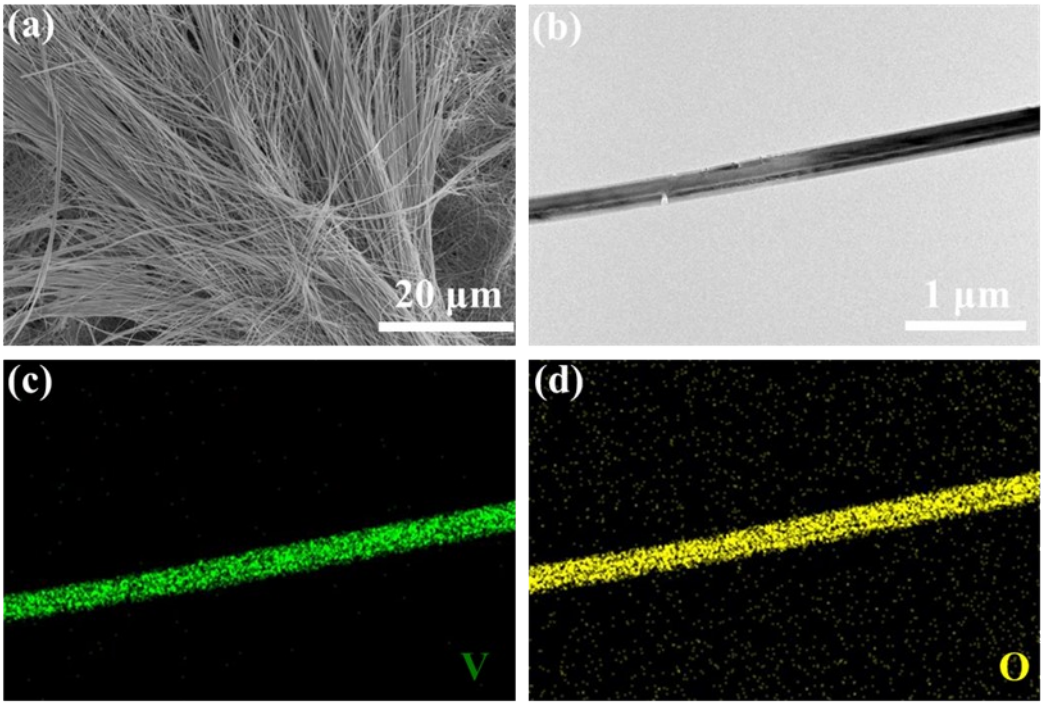

Fig. S1 (a) SEM image of B-VO_2. (b-d) HAADF-STEM images of B-VO_2 and corresponding elemental mapping of V and O.

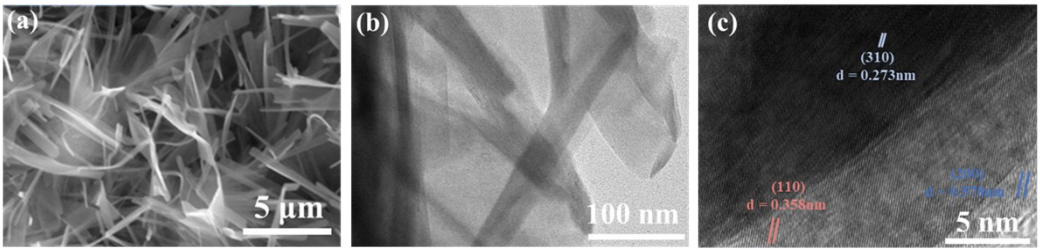

Fig. S2 (a-c) SEM, TEM, and HRTEM images of C-VO_2.

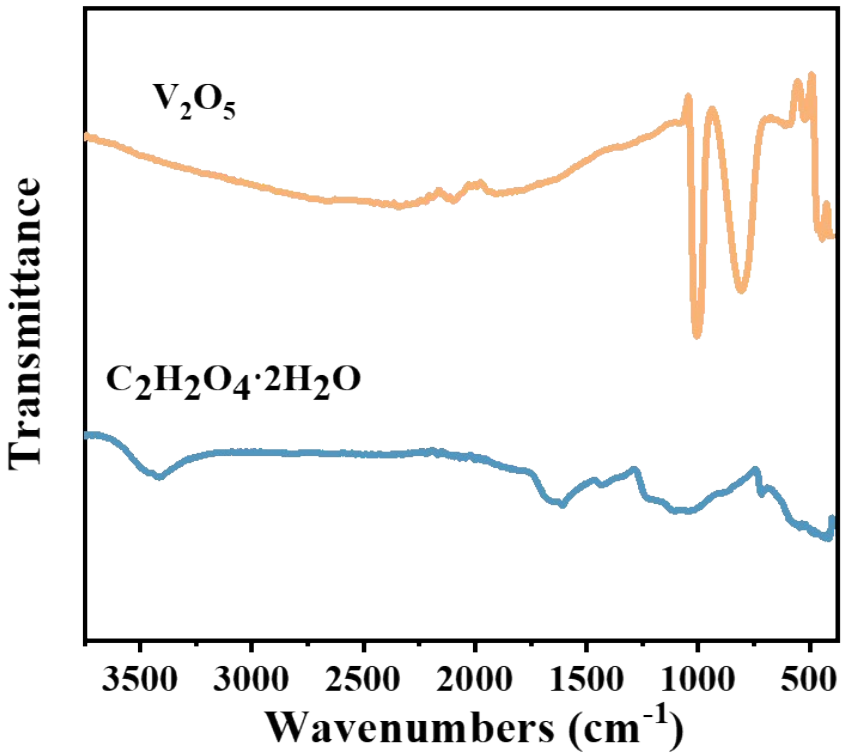

Fig. S3 FTIR spectra of V_2O_5 and $C_2H_2O_4 \cdot 2H_2O$.

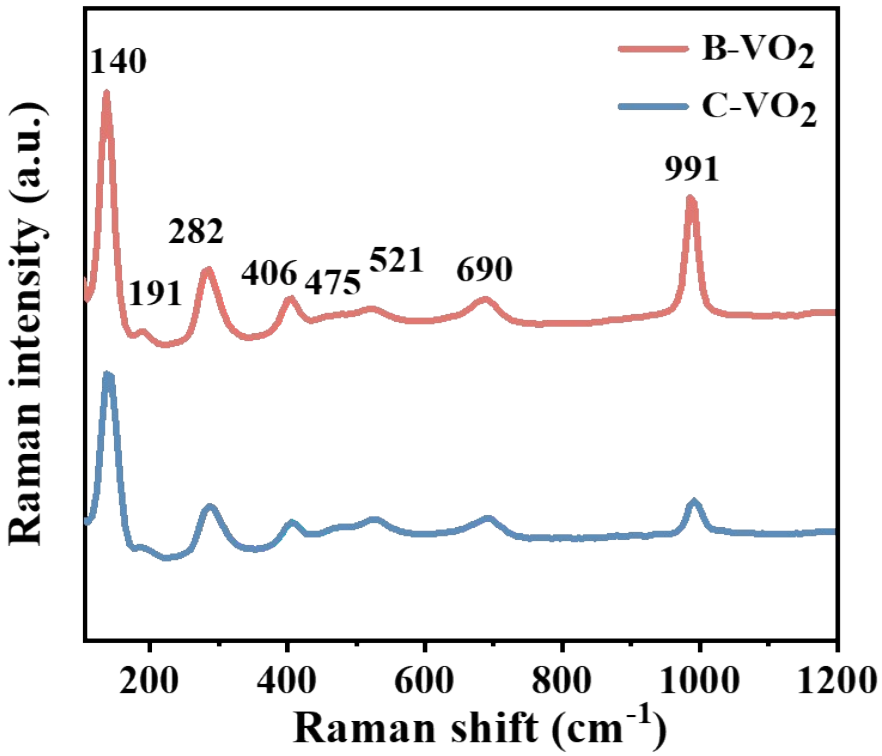

Fig. S4 Raman spectra of B-VO_2 and C-VO_2.

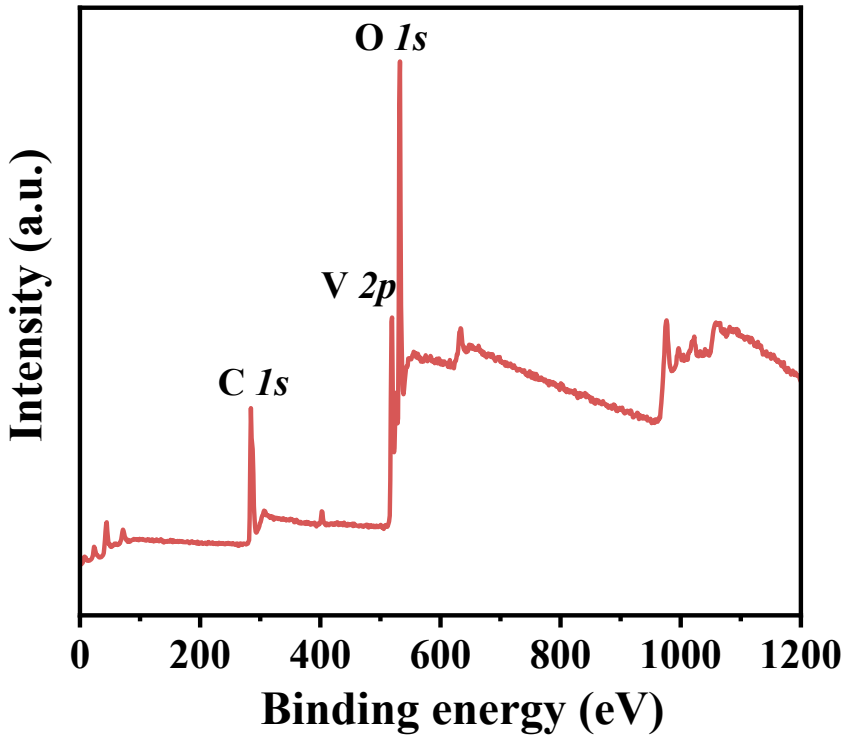

Fig. S5 XPS wide spectra of B-VO_2.

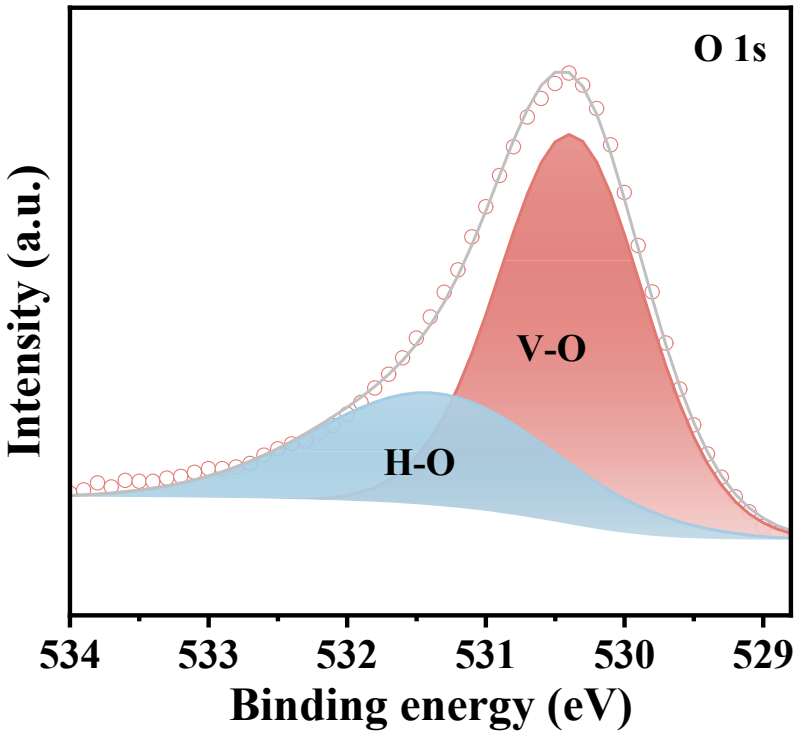

Fig. S6 XPS O 1s spectra of B-VO_2.

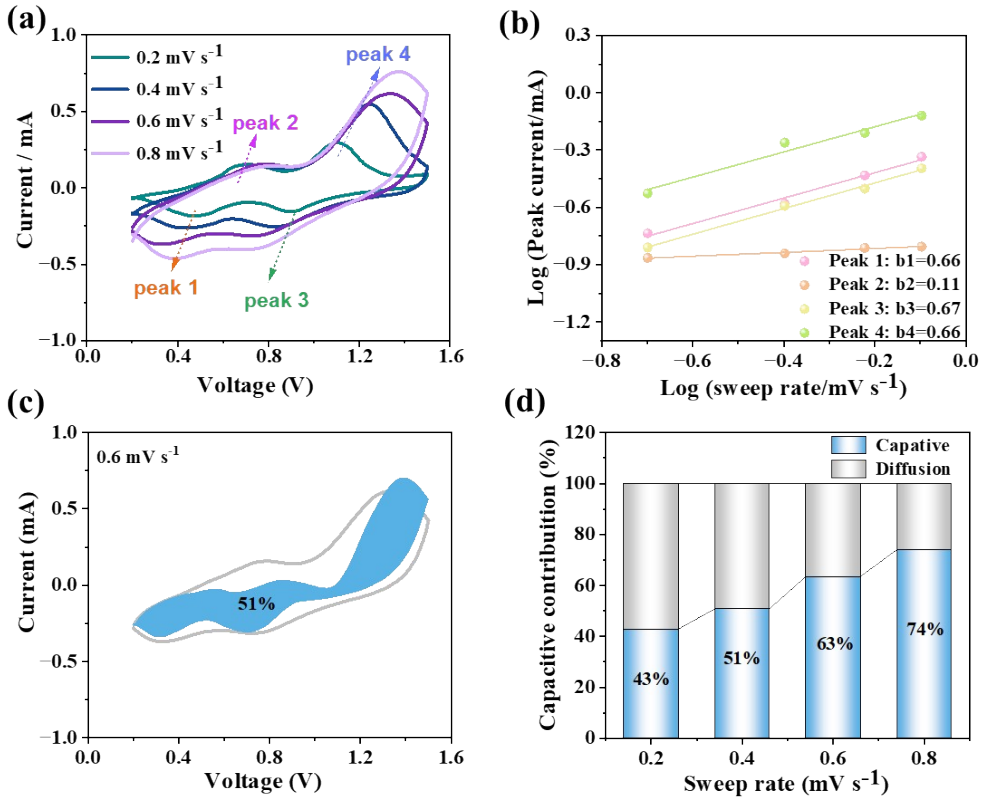

Fig. S7 (a) CV curves of C-VO_2 electrode at various scan rates; (b) log (peak current) versus log (sweep rate) plots according to the CV data at selected oxidation/reduction peaks; (c) CV curves of the C-VO_2 electrodes with capacity separation at 0.6 mV $s^{-1;}$ (d) The capacitive contributions of C-VO_2 electrode at different scan rates.

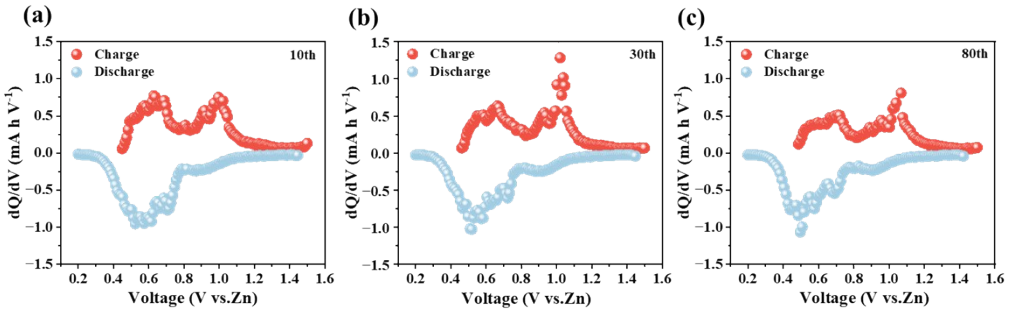

Fig. S8 dQ/dV curves of the B-VO_2 of (a) 10th, (b) 30th and (c) 80th cycle 0.2 A g^{-1}.

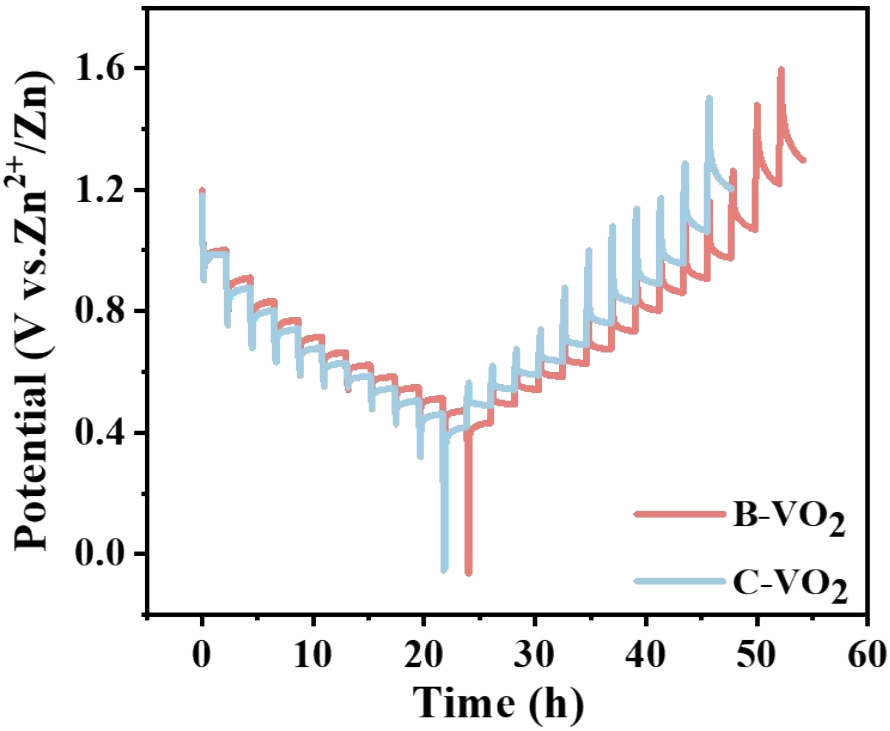

Fig. S9 Charge-discharge curves in the GITT measurement of B-VO_2 and C-VO_2 electrode at 0.2 A g^{-1}.

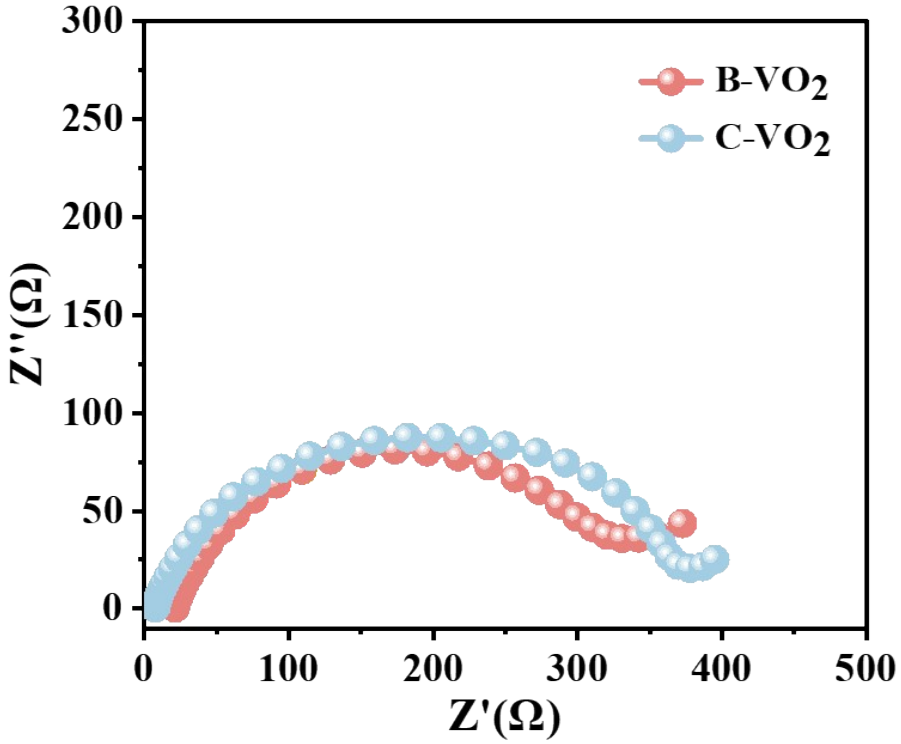

Fig. S10 EIS plots of the B-VO_2 and C-VO_2.

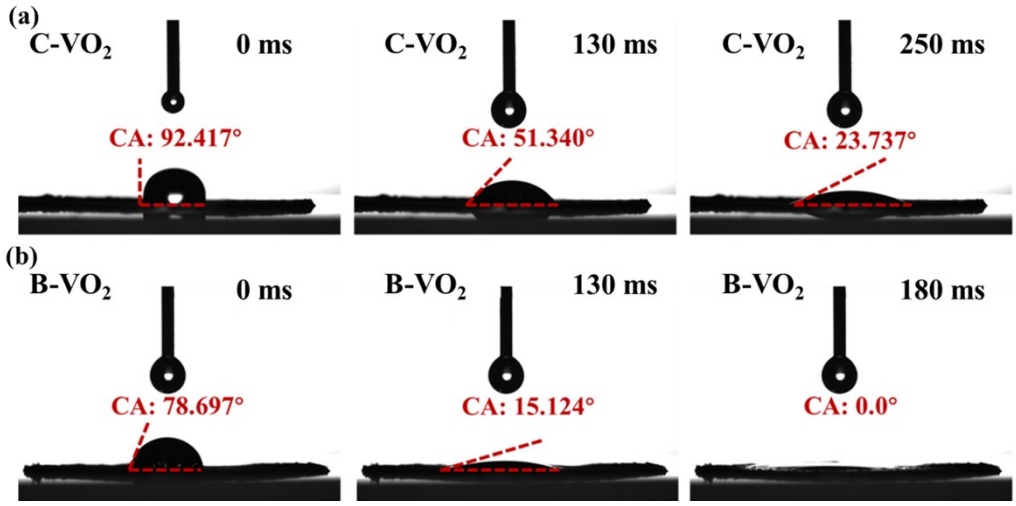

Fig. S11 Contact angle measurements of the $Zn(OTf)_2$ on the B-VO_2 and C-VO_2 electrode.

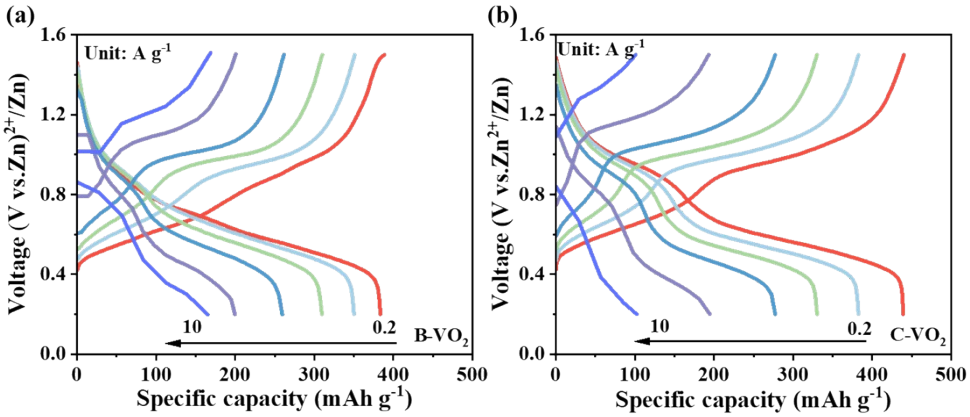

Fig. S12 GCD curves of electrode at different current densities: (a) B-VO_2, (b) C-VO_2.

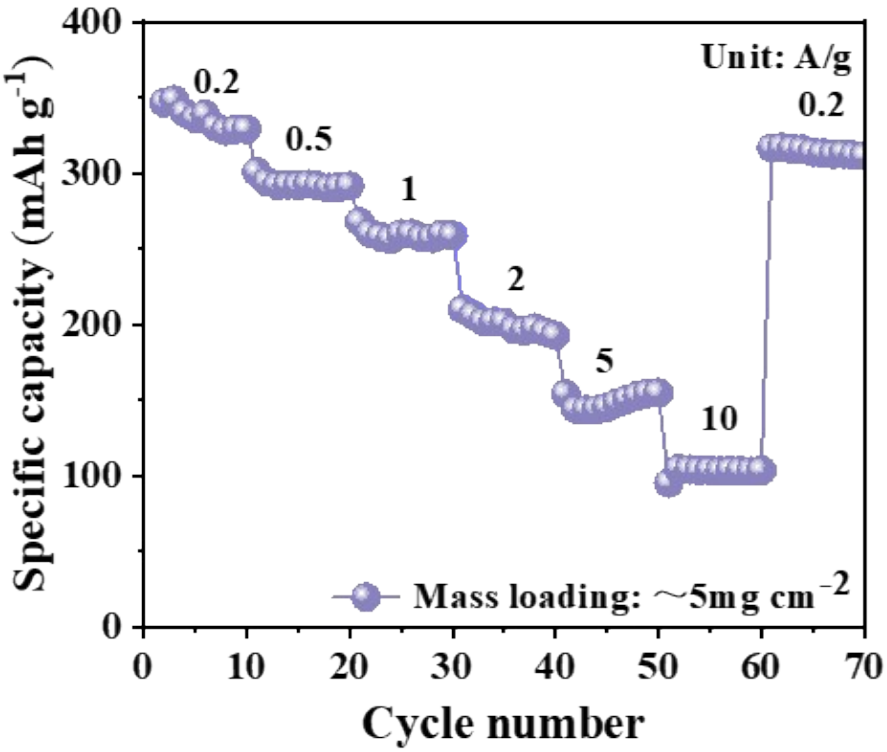

Fig. S13 Rate performance for B-$VO_2$with higher mass loading.

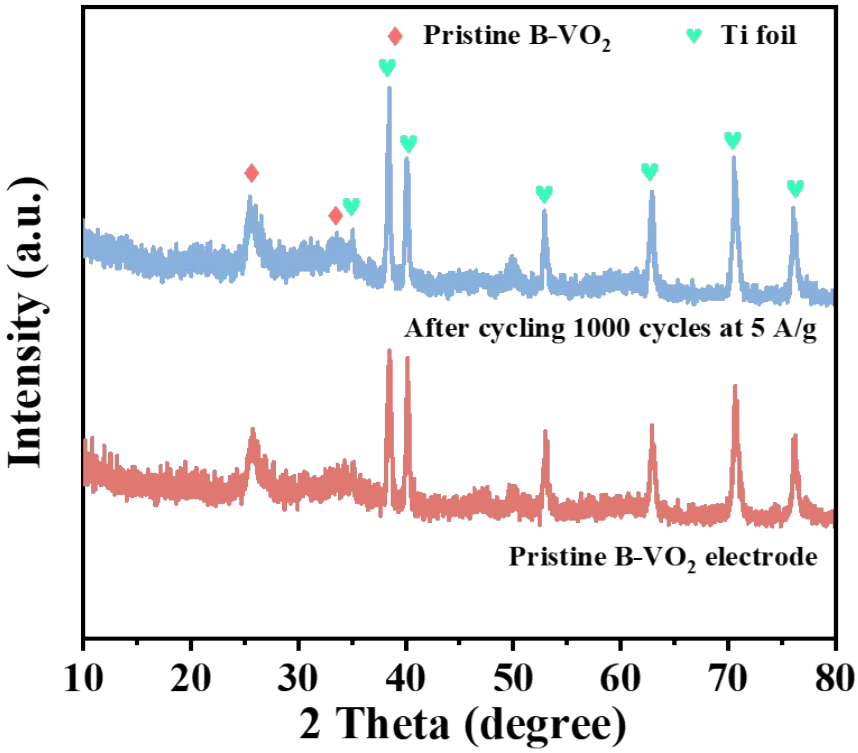

Fig. S14 XRD patterns of B-VO_2 electrodes under pristine and cycled states.

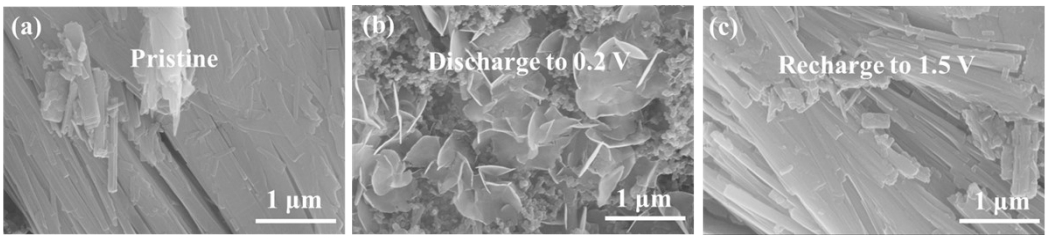

Fig. S15 SEM images of B-VO_2 Electrode at different charging/discharging states.

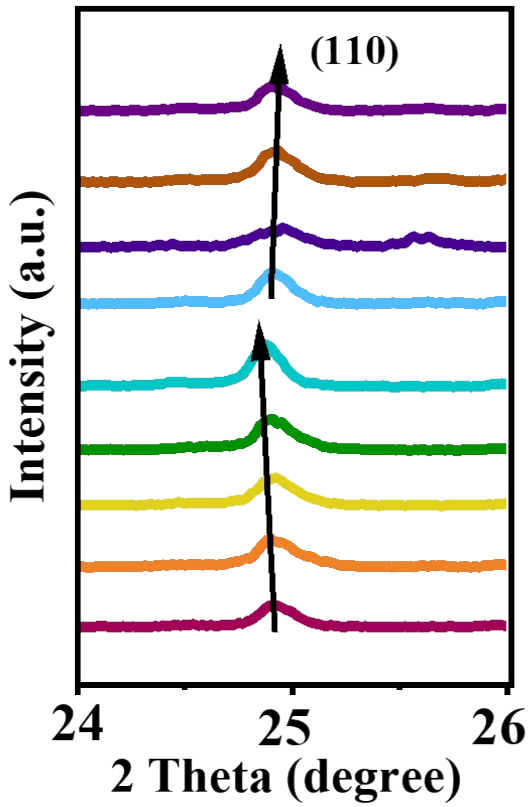

Fig. S16 Magnified view of the (110) peaks in Figure 5b.

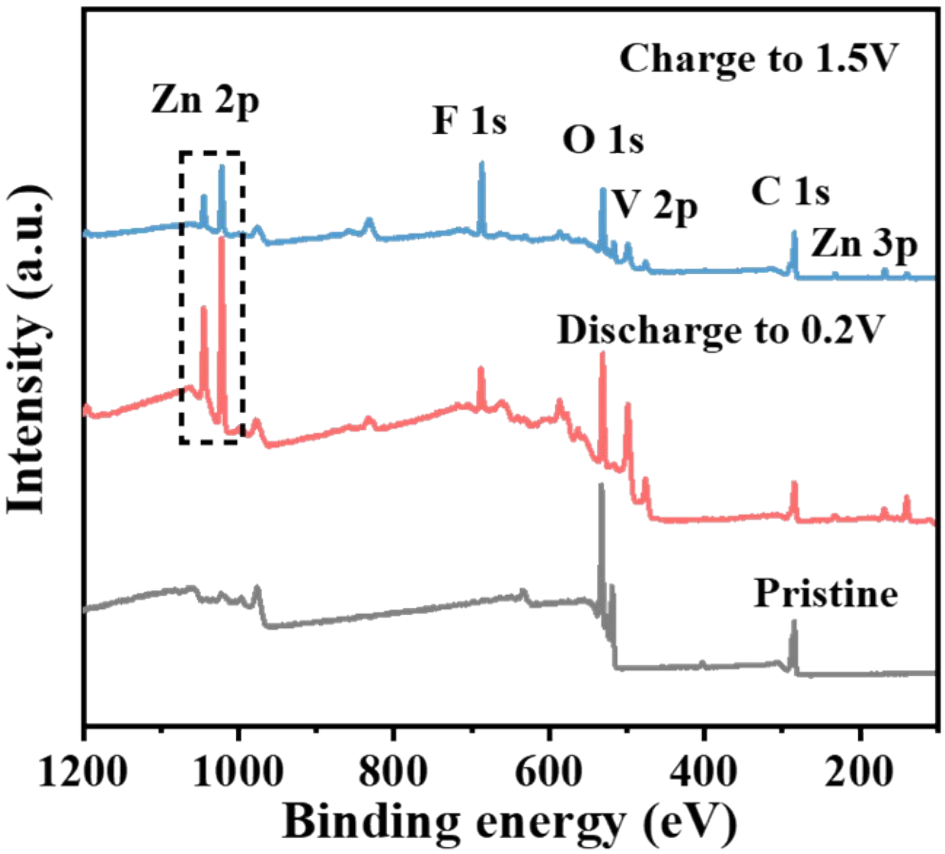

Fig. S17 XPS wide spectra of B-VO_2 electrode at different charge/discharge states.

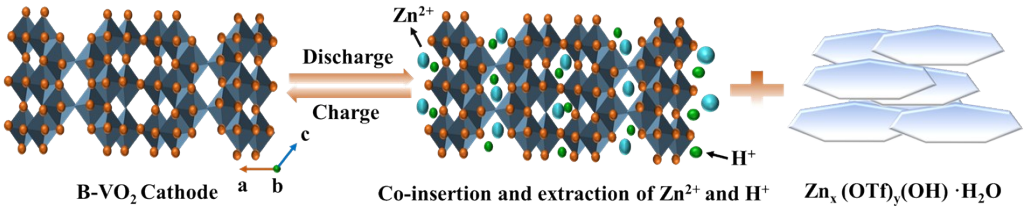

Fig. S18 Schematic diagram of the energy storage mechanism of B-VO_2.

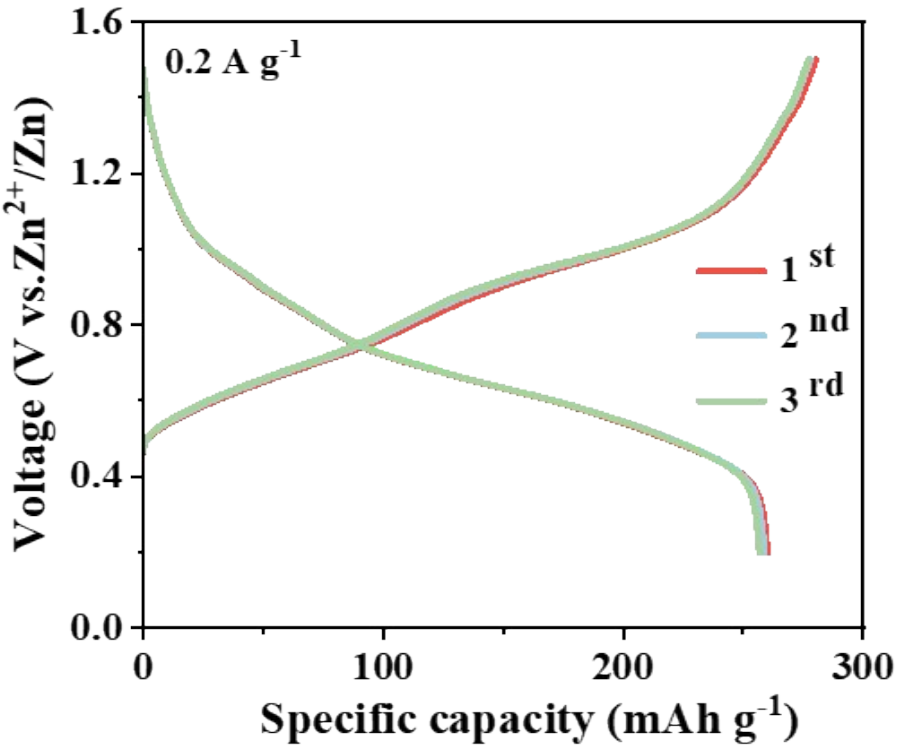

Fig. S19 The galvanostatic charge-discharge curves of Zn||B-VO_2 pouch cell at 0.2 A g^{-1}.

2. Supplementary Tables

Table S1 Comparison of Zn^{2+} diffusion coefficient for B-VO_2 and the previously reported vanadium-based cathodes in AZIBs.

Cathodes	D_{Zn} (cm^2 s^{-1})	References
V_2O_3	10^{-11}-10^{-13}	[1]
V_5O_{12}	10^{-9}-10^{-12}	[2]
$VN_{0.9}O_{0.15}$	10^{-11}-10^{-12}	[3]
KVO	10^{-9}-10^{-11}	[4]
PVSF-2/1	10^{-9}-10^{-11}	[5]
Mg-$NH_4V_4O_{10}$	10^{-10}-10^{-12}	[6]
VO_2- rGO	10^{-11}-10^{-13}	[7]
CVO	10^{-9}-10^{-11}	[8]
TOBI	10^{-11}-10^{-13}	[9]
VN-2	10^{-11}-10^{-13}	[10]
VO	10^{-11}-10^{-13}	[11]
B-VO_2	10^{-8}-10^{-10}	This work

Table S2 Comparison of electrochemical properties of B-VO_2 with previously reported vanadium-based cathodes in AZIBs.

Electrode materials	Specific capacity (mAh g^{-1} at A g^{-1})	Cycling stability	Reference
PVSF-2/1	398.9 (0.2)	78.5% at 5 A g^{-1} (2000)	[5]
CaVO	489.8 (0.1)	71% at 3 A g^{-1} (1000)	[12]
BNVO-3	384.9 (0.1)	92.9% at 3 A g^{-1} (1000)	[13]
S-NVOH	350 (0.3)	88% at 5 A g^{-1} (1300)	[14]
Na^+ doping VO_2	397 (0.2)	75% at 12 A g^{-1} (3000)	[15]
NaVO	427 (0.2)	74.3% at 2 A g^{-1} (1900)	[16]
G-VOH	386 (0.5)	86% at 2 A g^{-1} (1500)	[17]
VO	339 (0.2)	74% at 10 A g^{-1} (2000)	[18]
P-VO_2 @rGO	342 (0.1)	80% at 1 A g^{-1} (350)	[19]
Cr-doped VO_2 (B)	312.8 (0.1)	90% at 5 A g^{-1} (2000)	[20]
B-VO_2	357.6 (0.2)	86.1% at 5 A g^{-1} (4000)	This work

3. Theoretical calculation method

The density functional theory (DFT) calculations were carried out with the VASP code.[21] The Perdew-Burke-Ernzerhof (PBE) functional within generalized gradient approximation (GGA) was used to process the exchange-correlation, while the projectoraugmented-wave pseudopotential (PAW) was applied with a kinetic energy cut-off of 400 eV, which was utilized to describe the expansion of the electronic eigenfunctions.[22-23] All atomic positions were fully relaxed until energy and force reached a tolerance of 1×10^{-5} eV and 0.03 eV/Å, respectively. The dispersion corrected DFT-D3 method with the Becke–Johnson damping was employed to consider the long-range interactions[24-25]. Transition states along the reaction pathways and the activation energies were identified by the climbing image nudged elastic band (CI-NEB) method.[26]

4. References

[1] W. Ding, H. Y. Zheng, H. G. Gao, Q. N. Liu, Z. Hu, S. W. Wang, S. D. Wu, S. M. Fang, S. L. Chou, Adv. Energy Mater., 2021, **11,** 2100973.

[2] N. Zhang, M. Jia, Y. Y. Dong, J. Z. Xu, Y. C. Liu, L. F. Jiao, F. Y. Cheng, Adv. Funct. Mater., 2019, **29,** 1807331.

[3] J. W. Ding, Z. G. Du, B. Li, L. Z. Wang, S. W. Wang, Y. J. Gong, S. B. Yang, Adv. Mater., 2019, **31,** 1904369.

[4] B. Y. Tang, G. Z. Fang, J. Zhou, L. B. Wang, Y. P. Lei, C. Wang, T. Q. Lin, Y. Tang, S. Q. Liang, Nano Energy, 2018, **51,** 579-587.

[5] Y. Lu, S. Y. Han, J. G. Zheng, H. W. Zhao, H. Zhang, G. S. Jiang, L. X. Li, W. M. Zhou, B. G. An, C. G. Sun, ACS Appl. Mater. Interfaces., 2024, **17,** 1001-1013.

[6] H. Tang, F. Y. Chao, H. Y. Luo, K. S. Yu, J. Wang, H. B. Chen, R. M. Jia, F. Y. Xiong, Y. Q. Pi, P. Luo, Q. Y. An, ChemSusChem., 2023, **16,** e202300403.

[7] F. H. Cui, J. Zhao, D. X. Zhang, Y. Z. Fang, F. Hu, K. Zhu, Chem. Eng. J., 2020, **390,** 124118.

[8] H. J. Zeng, J. T. Huang, Y. B. Chen, L. Chen, H. Z. Wu, H. Y. Yang, Z. Chen, Tungsten, 2025, **7,** 547-556.

[9] F. X. Gao, H. G. Gao, K. Zhao, X. Y. Cao, J. W. Ding, S. W. Wang, J. Colloid Interface Sci., 2023, **629,** 928-936.

[10] Z. Y. Yuan, X. H. Yang, C. Y. Lin, P. X. Xiong, A. M. Su, Y. X. Fang, X. C. Chen, H. S. Fan, F. Y. Xiao, M. D. Wei, Q. R. Qian, Q. H. Chen, L. X. Zeng, J. Colloid Interface Sci., 2023, **640,** 487-497.

[11] W. Deng, Z. X. Xu, G. Li, X. L. Wang, Small, 2023, **19,** 2207754.

[12] T. Zhou, X. Du, G. Gao, J. Energy Chem. 2024, **95,** 9-19.

[13] Z. H. Deng, W. Shao, H. Y. Wang, Y. B. Wang, J. Sheng, H. C. Mu, L. Cheng, W. J. Wu, J. Power Sources, 2024, **614,** 234976.

[14] J. Zhang, M. S. Wang, M. Zeng, X. P. Li, L. Chen, Z. L. Yang, J. C. Chen, B. S. Guo, Z. Y. Ma, X. Li, J. Power Sources, 2021, **496,** 229832.

[15] Y. Liu, X. Wu, Nano Energy, 2021, **86,** 106124.

[16] G. Q. Jiang, J. C. Zhu, L. X. He, H. M. yang, N. Qiu, Y. Wang, Acta Mater., 2024, **277,** 120222.

[17] J. Zhang, M. S. Wang, J. L. Zhong, X. Wang, X. Z. Huang, Z. L. Yang, J. C. Chen, B. S. Guo,

Z. Y. Ma, X. Li, Mater. Chem. Front., 2021, **5,** 7518-7528.

[18] X. Y. Liu, L. Tao, L. Zhao, M. G. Ma, Z. Y. Liu, Z. Wang, Mater. Lett., 2024, **365,** 136462.

[19] J. H. Choi, J. S. Park, Y. C. Kang, Appl. Surf. Sci., 2022, **599,** 153890.

[20] X. H. Chen, X. Z. Zhai, Y. Q. Wu, X. Z. Wang, L. M. Zhang, C. Shang, H.W. Zhang, C.Z. Zhao, J. M. Shang, D. W. Liu, J. Energy Storage., 2025, **114,** 115826.

[21] G. Kresse, J. Furthmüller, Comp. Mater. Sci., 1996, **6,** 15-50.

[22] J. P. Perdew, K. Burke, M. Ernzerhof, Phys. Rev. Lett. 1996, **77,** 3865-3868.

[23] P. E. Blochl, Phys Rev B Condens Matter, 1994, **50,** 17953-17979.

[24] S. Grimme, J Comput Chem, 2006, **27,** 1787-1799.

[25] S. Grimme, S. Ehrlich, L. Goerigk, J. Comput. Chem., 2011, **32,** 1456-1465.

[26] G. Henkelman, B. P. Uberuaga, H. Jónsson, J. Chem. Phys., 2000, **113,** 9901-9904.